

Oxidized iron in garnets from the mantle transition zone

Ekaterina S. Kiseeva^{1*}, Denis M. Vasiukov^{2,3}, Bernard J. Wood¹, Catherine McCammon^{1,3}, Thomas Stachel⁴, Maxim Bykov^{1,3}, Elena Bykova^{1,3,5}, Aleksandr Chumakov^{1,6}, Valerio Cerantola⁶, Jeff W. Harris⁷ and Leonid Dubrovinsky³

The oxidation state of iron in Earth's mantle is well known to depths of approximately 200 km, but has not been characterized in samples from the lowermost upper mantle (200–410 km depth) or the transition zone (410–660 km depth). Natural samples from the deep (>200 km) mantle are extremely rare, and are usually only found as inclusions in diamonds. Here we use synchrotron Mössbauer source spectroscopy complemented by single-crystal X-ray diffraction to measure the oxidation state of Fe in inclusions of ultra-high pressure majoritic garnet in diamond. The garnets show a pronounced increase in oxidation state with depth, with $\text{Fe}^{3+}/(\text{Fe}^{3+} + \text{Fe}^{2+})$ increasing from 0.08 at approximately 240 km depth to 0.30 at approximately 500 km depth. The latter majorites, which come from pyroxenitic bulk compositions, are twice as rich in Fe^{3+} as the most oxidized garnets from the shallow mantle. Corresponding oxygen fugacities are above the upper stability limit of Fe metal. This implies that the increase in oxidation state is unconnected to disproportionation of Fe^{2+} to Fe^{3+} plus Fe^0 . Instead, the Fe^{3+} increase with depth is consistent with the hypothesis that carbonated fluids or melts are the oxidizing agents responsible for the high Fe^{3+} contents of the inclusions.

The Earth's peridotitic upper mantle contains about 6.3wt% Fe¹ predominantly stored as Fe²⁺ in the main rock-forming minerals: olivine, pyroxene, spinel and garnet. Analyses of these minerals from peridotite xenoliths and less abundant mantle pyroxenites using Mössbauer spectroscopy indicate that the Fe³⁺ content of fertile upper mantle is very low with $\text{Fe}^{3+}/(\text{Fe}^{3+} + \text{Fe}^{2+}) \sim 0.036^2$. In the case of ferric iron, spinel is a major host in the uppermost mantle and the Fe³⁺ contents of this mineral are sufficiently high to be used to calculate the oxygen fugacity (f_{O_2}) recorded by mantle peridotites using the olivine–orthopyroxene–spinel oxybarometer³. The results indicate that the subcontinental lithospheric upper mantle exhibits oxygen fugacities that are close to the reference FMQ (fayalite–magnetite–quartz buffer)^{3,4}, whereas peridotites from close to subduction zones are about 1 log f_{O_2} unit higher and suboceanic peridotites about 1 log unit lower than FMQ². At pressures above 2.8 GPa, spinel is replaced by garnet as the aluminous phase in peridotite. Mössbauer data on xenoliths from deeper parts of the lithosphere⁵ indicate a general increase in $\text{Fe}^{3+}/(\text{Fe}^{2+} + \text{Fe}^{3+})$ of garnet with depth, with values of around 0.04 (corresponding to about 100 km depth), while at 200 km depth this ratio is ~ 0.1 . When translated to oxygen fugacity, however, these results indicate a decline relative to FMQ with depth because of the increased stability of ferric iron in garnet at high pressure⁶. Extrapolation of the data to higher pressures implies that the Fe–FeO (iron–wüstite, IW) buffer curve could be crossed in the mantle at depths below 250 km^{5,7}, leading to the possibility of Fe-rich metal being stabilized in the mantle transition zone. This is an important suggestion, consistent with observations of Fe-rich metallic inclusions in diamond from depths of the base of the lithospheric mantle^{8,9} and >360 km¹⁰. Similar deep diamonds contain inclusions of majoritic garnet, the

major silicate inclusion from the transition zone. Given the role of garnet as a key host for Fe³⁺ in the upper mantle, it is important to determine how the Fe³⁺ contents and oxygen fugacities recorded by garnet inclusions in diamond from depths >250 km relate to those derived from upper-mantle xenoliths (from <200 km) and to the apparent stability of Fe-rich alloys and other indicators of ultra-reduced conditions¹¹ in some very-high-pressure assemblages. The purpose of our study was, therefore, to determine how the oxidation state of iron in garnet (included in diamond) from the mantle varies as a function of depth and to translate measured oxidation states to oxygen fugacities.

Sample analysis. To determine the oxidation state of Fe in garnet inclusions in diamond, we used single-crystal X-ray diffraction (XRD) analysis (beamline P02 at PETRA III, Hamburg) combined with synchrotron Mössbauer source (SMS) spectroscopy (beamline ID18 at the European Synchrotron Radiation Facility, Grenoble). The diamonds were polished to expose the garnet before analysis. We obtained spectra (Supplementary Figs. 1–2 and Supplementary Table 1) of 13 small (0.1–0.3 mm in diameter) majoritic inclusions in diamonds from the Jagersfontein kimberlite (South Africa) (Supplementary Fig. 3). The inclusions were initially studied by XRD and confirmed as predominantly monophase garnet single crystals or (in very few cases) as aggregates of single crystals (Supplementary Tables 2–3). There is good agreement between determinations of $\text{Fe}^{3+}/(\text{Fe}^{2+} + \text{Fe}^{3+})$ using Mössbauer spectroscopy and single-crystal X-ray refinement as well as with calculations based on the composition assuming stoichiometry (Supplementary Table 4). In several samples an unexpectedly high content of ferric iron was detected (up to $\sim 30\%$ of total iron) and requires further detailed consideration.

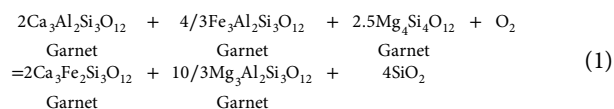
¹Department of Earth Sciences, University of Oxford, Oxford, UK. ²Laboratory of Crystallography, University of Bayreuth, Bayreuth, Germany. ³Bayerisches Geoinstitut, University of Bayreuth, Bayreuth, Germany. ⁴Department of Earth and Atmospheric Sciences, University of Alberta, Edmonton, Alberta, Canada. ⁵DESY Photon Science, Hamburg, Germany. ⁶ESRF–The European Synchrotron, Grenoble, France. ⁷School of Geographical and Earth Sciences, University of Glasgow, Glasgow, UK. *e-mail: kate.kiseeva@earth.ox.ac.uk

Source lithology of majorites and their ferric iron content. In the commonest case of a single garnet inclusion there is no unique geobarometer that enables pressure to be unequivocally determined. However, at pressures beyond 7.5 GPa coexisting pyroxene dissolves progressively into garnet as the majoritic components (Mg,Fe) $_4\text{Si}_4\text{O}_{12}$ and $\text{Na}_2\text{MgSi}_5\text{O}_{12}$. The concentrations of these components in majoritic garnet give an equilibrium pressure, provided that pyroxene is present in the source¹². In the absence of pyroxene in the source, the derived pressure is a minimum estimate. In subducted basaltic lithologies the pyroxene-to-garnet transformation produces a garnetite of ~95% majoritic garnet and ~5% stishovite at about 500 km depth^{13,14}, whereas in rocks with peridotitic composition majoritic garnet forms a biminerallitic rock with the high-pressure form of (Mg,Fe) $_2\text{SiO}_4$ (wadsleyite or ringwoodite)¹⁵. There are, however, significant compositional differences between garnets from the two end-member lithologies, with the (Mg,Fe) $_4\text{Si}_4\text{O}_{12}$ substitution dominating in peridotitic rocks while basaltic or eclogitic compositions produce garnet with considerable amounts of the $\text{Na}_2\text{MgSi}_5\text{O}_{12}$ component (Fig. 1). Perhaps surprisingly, the compositions of most inclusions from diamond seem to come from a third rock type, pyroxenite, which is intermediate in composition between peridotite and eclogite¹⁶. Pyroxenite lenses are common in mantle peridotites¹⁷ and are considered to be produced by reactions between peridotitic and eclogitic compositions, possibly through the agency of carbonated melts^{18,19}. Although following the 'peridotitic' trend of Fig. 1, pyroxenitic garnets are lower in Cr_2O_3 and Mg\# ($\text{Mg}/(\text{Mg}+\text{Fe})$) and higher in CaO than peridotitic garnets. The garnet inclusions we have studied are (in common with most other majorite inclusions) pyroxenitic in composition, in that they follow the peridotite trend on a plot of divalent cations (M^{2+}) versus ($\text{M}^{4+}+\text{M}^{5+}$) (Fig. 1), but are low in Cr_2O_3 (0.03–0.34 wt%) and Mg\# (0.65–0.81) and high in CaO (4.62–11.2 wt%). As far as we are aware, no majoritic garnets of peridotitic composition have yet been reported as inclusions in diamond from the mantle transition zone. This implies a genetic connection, explored in more detail

elsewhere^{18,19} between the minor mantle rock type pyroxenite, and the diamond host.

Our measurements show an increase in $\text{Fe}^{3+}/(\text{Fe}^{2+}+\text{Fe}^{3+})$ with increasing amount of majorite substitution and hence pressure (Fig. 2). Assuming the presence of pyroxene in the pyroxenitic diamond substrates, garnet compositions yield pressures of formation of 7.7–17.9 GPa using the Beyer–Frost majorite geobarometer¹². These are minimum pressures, however, because majoritic garnet equilibrium with pyroxene has not been demonstrated in our samples. Interestingly, Fig. 2 shows that $\text{Fe}^{3+}/(\text{Fe}^{2+}+\text{Fe}^{3+})$ is extremely well correlated with calculated pressure, increasing from 0.08 at 7.7 GPa to values between 0.30 at 16 GPa and 0.27 at 18 GPa. Note that at least 3 of these 13 garnets were formed at (minimum) pressures of 13–18 GPa and, therefore crystallized in the transition zone (410–660 km depth). It is also interesting to note that our measured $\text{Fe}^{3+}/(\text{Fe}^{2+}+\text{Fe}^{3+})$ values define a clear extension of the trend that is apparent in the data from peridotite xenoliths crystallized at lower pressures, and that Fe from the transition zone garnets is at least twice as oxidized as in any garnet from xenoliths of subcratonic lithospheric mantle.

Oxygen fugacity in the mantle transition zone. To estimate the oxygen fugacities represented by these Fe^{3+} -bearing inclusions we looked for the simplest equilibrium available containing the fewest number of activities undefined by garnet composition:



In this case we need to define the activity of SiO_2 , which we assumed was slightly (0.01 log units) above the forsterite–enstatite equilibrium and hence consistent with the garnets being close to equilibrium with peridotite. Although we recognize that this is a

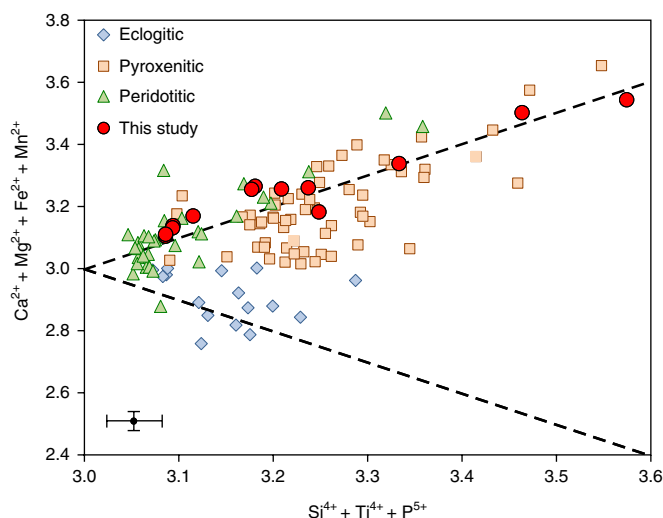


Fig. 1 | Chemical composition of majoritic garnet inclusions in diamonds worldwide. Literature data are from ref. ¹⁶; all values are in cations per 12-oxygen formula unit. Inclusions studied here are from the Jagersfontein kimberlite. To compare compositions with those of previous studies, all iron has been calculated as Fe^{2+} . Uncertainties are estimated at 1% relative to the measured value for microprobe analysis and shown as indicative error bars. Dashed lines delineate peridotitic (upper) and eclogitic (lower) trends (for explanation see ref. ¹⁶).

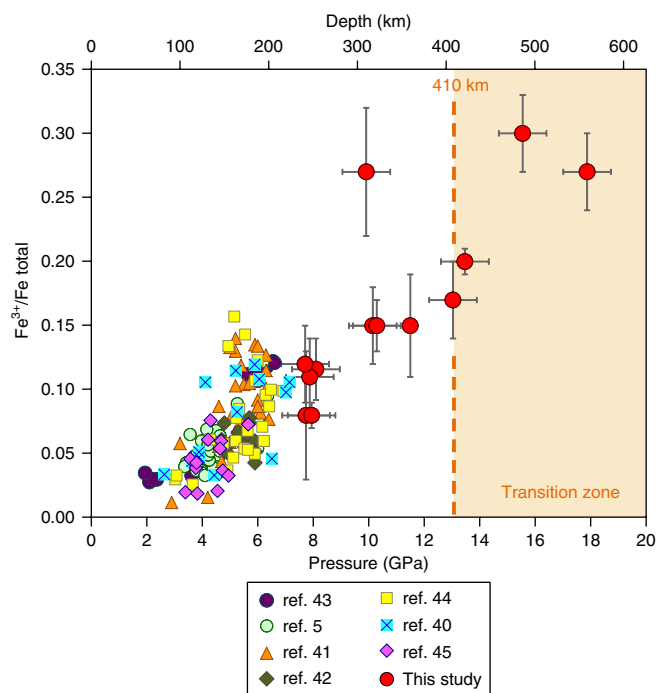
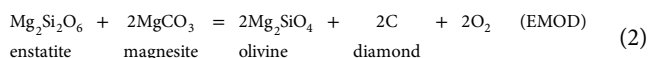


Fig. 2 | Ferric iron contents of majoritic garnets from Jagersfontein diamonds compared with lithospheric garnets from peridotite xenoliths. All ferric iron contents were determined by Mössbauer spectroscopy^{5,27–32}. The uncertainty in pressure calculations (0.86 GPa) was taken from ref. ¹².

crude assumption, we show below that it yields (correctly) oxygen fugacities that are consistent with the stability of metallic Fe in experiments performed in iron capsules on similar compositions²⁰. We took thermodynamic data for equilibrium (1) from a published database^{21,22} and calculated oxygen fugacities for pressures given by the Beyer–Frost geobarometer¹² at temperatures corresponding to a mantle adiabat with a potential temperature of 1,350 °C²³ (Methods). Results (Fig. 3) indicate that the analysed garnets correspond to oxygen fugacities from $\sim 0.26 \log f_{\text{O}_2}$ units below to about $3 \log f_{\text{O}_2}$ units above the IW buffer, implying that they were not in equilibrium with Fe metal and not oxidized by disproportionation of Fe^{2+} to Fe^{3+} plus Fe^0 (Methods). We checked our calculation method and assumptions using data from experiments in which garnets were synthesized in equilibrium with Fe metal and their Fe^{3+} contents measured²⁰. In this case (Fig. 3), 4 of the 5 experiments give calculated oxygen fugacities, as expected, just below Fe–FeO equilibrium. This test indicates that our methods are reasonably accurate and our conclusions justified, although uncertainties in activity expressions imply about 1 log unit of uncertainty in absolute f_{O_2} (Methods). Note that any actual error in activity expressions would lead to all points moving in the same direction, thus preserving the trends of Fig. 3.

Since Fe^{2+} disproportionation seems not to be responsible, the source of the oxidizing agent that generated the high $\text{Fe}^{3+}/(\text{Fe}^{2+} + \text{Fe}^{3+})$ ratios of the transition zone garnets is of considerable interest. It has previously been suggested that the pyroxenite substrates in which the garnets and their host diamonds crystallized were generated by reactions between subducted eclogite and peridotite aided by carbonate melt^{18,19} and that diamond and oxidized majoritic garnet are products of this interaction. For this reason we compare our results (Fig. 3) to a carbon–carbonate equilibrium that is relevant to the deeper upper mantle:



We used tabulated thermodynamic data^{21,22} and corrected for the effect of the phase change from olivine to wadsleyite at ~ 13 GPa. Figure 3 shows that our inclusions are in the (reduced) diamond stability field and that they approach EMOD with increasing pressure, which means that oxidation of Fe^{2+} during the reduction of carbonate in a fluid or melt phase is a plausible mechanism for generating the Fe^{3+} present in the garnets, as also suggested in a recent study²⁴. The inclusions have $\delta^{18}\text{O}_{\text{VSMOW}}$ values between +8.6 and +10‰²⁵, consistent with a protolith that contains a substantial proportion of subducted oceanic crust, although it is no longer eclogitic. The light rare-earth element (LREE)-depleted and fairly flat chondrite-normalized middle–heavy REE patterns²⁶ of the majoritic garnet inclusions suggest that during subduction, their protolith was chemically depleted in incompatible trace elements, including LREEs, during partial melting in the garnet stability field.

In conclusion, we have shown that, in the upper mantle and transition zone, there is a systematic increase with depth in the oxidation state of iron in garnet from pyroxenitic bulk compositions. Although the volumetric proportion of pyroxenite in this part of the mantle is unknown, we note that these are the only available garnet inclusions that demonstrably come from the mantle transition zone and are hence the only indication of oxygen fugacity and oxidation states in this region of the mantle. The deepest samples (from ~ 500 km depth) have $\text{Fe}^{3+}/(\text{Fe}^{3+} + \text{Fe}^{2+})$ of 0.30, more than double the ferric iron content of any garnet from the shallower (< 200 km) peridotitic mantle. These ferric iron contents correspond to oxygen fugacities above the IW buffer, which means that the high Fe^{3+} contents were not generated by disproportionation of Fe^{2+} to Fe^{3+} and Fe^0 . With increasing depth relative oxygen fugacities increase and

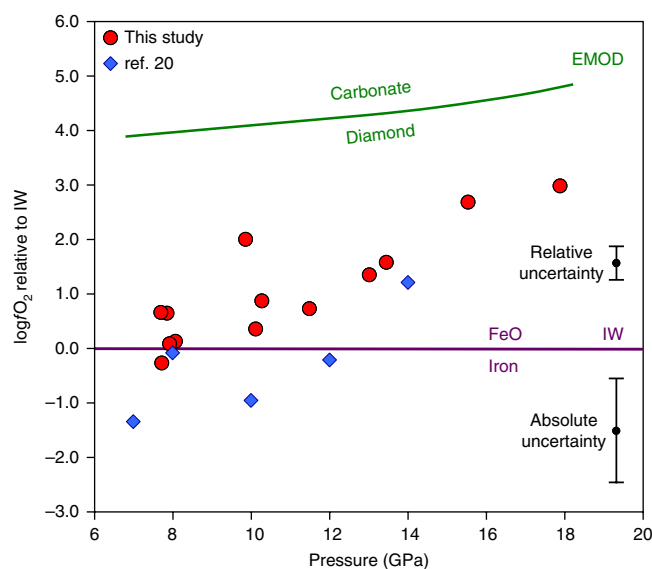


Fig. 3 | Calculated oxygen fugacities (see Methods) of the majoritic inclusions and of garnets crystallized in coexistence with Fe metal²⁰.

The data are plotted relative to the EMOD and Fe–FeO (IW) buffers. Uncertainty in absolute oxygen fugacity is estimated at ± 1 log unit with relative uncertainty approximately ± 0.3 log units (Methods).

approach the carbon–carbonate equilibrium, suggesting that carbonate was the oxidizing agent responsible for generating the high Fe^{3+} of these mantle garnets.

Methods

Methods, including statements of data availability and any associated accession codes and references, are available at <https://doi.org/10.1038/s41561-017-0055-7>.

Received: 10 April 2017; Accepted: 14 December 2017;

Published online: 22 January 2018

References

- McDonough, W. F. & Sun, S. S. The Composition of the Earth. *Chem. Geol.* **120**, 223–253 (1995).
- Canil, D. et al. Ferric iron in peridotites and mantle oxidation states. *Earth Planet. Sci. Lett.* **123**, 205–220 (1994).
- Wood, B. J., Bryndzia, L. T. & Johnson, K. E. Mantle oxidation state and its relationship to tectonic environment and fluid speciation. *Science* **248**, 337–345 (1990).
- Frost, D. J. & McCammon, C. A. The redox state of Earth's mantle. *Annu. Rev. Earth Planet. Sci.* **36**, 389–420 (2008).
- Woodland, A. B. & Koch, M. Variation in oxygen fugacity with depth in the upper mantle beneath the Kaapvaal craton, Southern Africa. *Earth Planet. Sci. Lett.* **214**, 295–310 (2003).
- Gudmundsson, G. & Wood, B. J. Experimental tests of garnet peridotite oxygen barometry. *Contrib. Mineral. Petrol.* **119**, 56–67 (1995).
- Ballhaus, C. Is the upper mantle metal-saturated. *Earth Planet. Sci. Lett.* **132**, 75–86 (1995).
- Jacob, D. E., Kronz, A. & Viljoen, K. S. Cohenite, native iron and troilite inclusions in garnets from polycrystalline diamond aggregates. *Contrib. Mineral. Petrol.* **146**, 566–576 (2004).
- Sobolev, N. V., Efimova, E. S. & Pospelova, L. N. Native iron in diamonds of Yakutia and its paragenesis. *Geol. Geofiz.* **22**, 25–28 (1981).
- Smith, E. M. et al. Large gem diamonds from metallic liquid in Earth's deep mantle. *Science* **354**, 1403–1405 (2016).
- Golubkova, A., Schmidt, M. W. & Connolly, J. A. D. Ultra-reducing conditions in average mantle peridotites and in podiform chromitites: A thermodynamic model for moissanite (SiC) formation. *Contrib. Mineral. Petrol.* **171**, 1–17 (2016).
- Beyer, C. & Frost, D. J. The depth of sub-lithospheric diamond formation and the redistribution of carbon in the deep mantle. *Earth Planet. Sci. Lett.* **461**, 30–39 (2017).

13. Irifune, T. & Ringwood, A. E. in *High-pressure Research in Mineral Physics* Vol. 1 (eds Manghnani, M. H. & Syono, Y.) 235–246 (Terra Scientific, Tokyo, 1987).
14. Wood, B. J., Kiseeva, E. S. & Matzen, A. K. Garnet in the Earth's Mantle. *Elements* **9**, 421–426 (2013).
15. Irifune, T. & Ringwood, A. E. Phase transformations in a harzburgite composition to 26 GPa—implications for dynamical behavior of the subducting slab. *Earth Planet. Sci. Lett.* **86**, 365–376 (1987).
16. Kiseeva, E. S. et al. Metapyroxenite in the mantle transition zone revealed from majorite inclusions in diamonds. *Geology* **41**, 883–886 (2013).
17. Pearson, D. G., Davies, G. R. & Nixon, P. H. Geochemical constraints on the petrogenesis of diamond facies pyroxenites from the Beni Bousera peridotite massif, North Morocco. *J. Petrol.* **34**, 125–172 (1993).
18. Kiseeva, E. S., Wood, B. J., Ghosh, S. & Stachel, T. The pyroxenite–diamond connection. *Geochem. Perspect. Lett.* **2**, 1–9 (2016).
19. Thomson, A. R., Walter, M. J., Kohn, S. C. & Brooker, R. A. Slab melting as a barrier to deep carbon subduction. *Nature* **529**, 76–79 (2016).
20. Rohrbach, A. et al. Metal saturation in the upper mantle. *Nature* **449**, 456–458 (2007).
21. Holland, T. J., Hudson, N. F., Powell, R. & Harte, B. New thermodynamic models and calculated phase equilibria in NCFMAS for basic and ultrabasic compositions through the transition zone into the uppermost lower mantle. *J. Petrol.* **54**, 1901–1920 (2013).
22. Holland, T. J. B. & Powell, R. An improved and extended internally consistent thermodynamic dataset for phases of petrological interest, involving a new equation of state for solids. *J. Metamorph. Geol.* **29**, 333–383 (2011).
23. Mckenzie, D. & Bickle, M. J. The volume and composition of melt generated by extension of the lithosphere. *J. Petrol.* **29**, 625–679 (1988).
24. Xu, C. et al. Recovery of an oxidized majorite inclusion from Earth's deep asthenosphere. *Sci. Adv.* **3**, e1601589 (2017).
25. Ickert, R. B., Stachel, T., Stern, R. A. & Harris, J. W. Extreme ^{18}O -enrichment in majorite constrains a crustal origin of transition zone diamonds. *Geochem. Perspect. Lett.* **1**, 65–74 (2015).
26. Tappert, R. et al. Diamonds from Jagersfontein (South Africa): Messengers from the sublithospheric mantle. *Contrib. Mineral. Petrol.* **150**, 505–522 (2005).
27. Canil, D. & O'Neill, H. S. C. Distribution of ferric iron in some upper-mantle assemblages. *J. Petrol.* **37**, 609–635 (1996).
28. Goncharov, A. G., Ionov, D. A., Doucet, L. S. & Pokhilenko, L. N. Thermal state, oxygen fugacity and C–O–H fluid speciation in cratonic lithospheric mantle: new data on peridotite xenoliths from the Udachnaya kimberlite, Siberia. *Earth Planet. Sci. Lett.* **357**, 99–110 (2012).
29. Lazarov, M., Woodland, A. B. & Brey, G. P. Thermal state and redox conditions of the Kaapvaal mantle: A study of xenoliths from the Finsch mine, South Africa. *Lithos* **112**, 913–923 (2009).
30. Luth, R. W., Virgo, D., Boyd, F. R. & Wood, B. J. Ferric iron in mantle-derived garnets—implications for thermobarometry and for the oxidation state of the mantle. *Contrib. Mineral. Petrol.* **104**, 56–72 (1990).
31. McCammon, C. & Kopylova, M. G. A redox profile of the Slave mantle and oxygen fugacity control in the cratonic mantle. *Contrib. Mineral. Petrol.* **148**, 55–68 (2004).
32. Kopylova, M. G., Beausoleil, Y., Goncharov, A., Burgess, J. & Strand, P. Spatial distribution of eclogite in the Slave cratonic mantle: the role of subduction. *Tectonophysics* **672**, 87–103 (2016).

Acknowledgements

We thank T. Holland for checking some of our calculations and D. Frost for providing his spreadsheet for oxygen fugacity calculations using garnet equilibria, A. Schönleber for discussion of XRD results and D. Simonova for assistance during Mössbauer experiments. We acknowledge support from European Research Council grant 267764 to B.J.W. and NERC grant NE/L010828/1 to E.S.K. Financial support was provided to L.D. and C.M. through DFG grants Mc 3/18-1 and Mc 3/20-1, and through BMBF grants. We acknowledge the European Synchrotron Radiation Facility for provision of synchrotron radiation facilities.

Author contributions

Work was initiated and planned by E.S.K. and L.D. T.S. and J.W.H. provided the samples and their detailed description. M.B., D.M.V., E.B. and L.D. performed the X-ray diffraction measurements. D.M.V., M.B., E.B. and L.D. processed and analysed the diffraction data. D.M.V., V.C., A.C. and C.M. collected, processed and analysed the Mössbauer spectra. E.S.K. and B.J.W. interpreted the data, performed the thermodynamic calculations and prepared the manuscript. All co-authors read, commented and approved of the manuscript.

Competing interests

The authors declare no competing financial interests.

Additional information

Supplementary information is available for this paper at <https://doi.org/10.1038/s41561-017-0055-7>.

Reprints and permissions information is available at www.nature.com/reprints.

Correspondence and requests for materials should be addressed to E.S.K.

Publisher's note: Springer Nature remains neutral with regard to jurisdictional claims in published maps and institutional affiliations.

Methods

Samples. The garnet inclusions in diamonds investigated in this study originate from the Jagersfontein kimberlite in South Africa (more details about the host diamonds, compositions, REE patterns and so on are given in ref.²⁰). The inclusions were released by crushing the host diamonds, mounted in epoxy disks with 0.7 mm thickness supported by brass rings and then polished. All measurements described here were performed on the samples mounted in epoxy. The size of the inclusions studied varied from about 60 µm in diameter and 20 µm thick to 300 µm in lateral dimensions and about 300 µm thickness.

Mössbauer spectroscopy. Mössbauer absorption spectra were collected at ambient temperature at the Nuclear Resonance beamline (ID18) at the European Synchrotron Radiation Facility (Grenoble) using an SMS³³. The experiment was conducted in transmission geometry and folded spectra contained 512 channels. The typical beam size was 16 × 20 µm² full width at half maximum (FWHM). The line width of the SMS was determined before and after collection of each spectrum of the sample by measuring the reference single line absorber (K₂Mg⁵⁷Fe(CN)₆). More information about sample mounting and alignment procedure is given in ref.³⁴. Each spectrum was collected for 4 to 12 h.

The Mössbauer spectra were fitted using MossA software³⁵ version 1.01a with the full transmission integral assuming a Lorentzian-squared line shape of the SMS. The fitted parameters were centre shift (CS), FWHM, intensity (area), quadrupole splitting (QS) and component intensity ratio of the main doublet (*a*₁₂, where the asymmetry is due to the Goldanskii–Karyagin effect for iron located in the distorted cubic *X* position of the garnet structure, see ref.³⁶; there is no effect for iron in the octahedral *Y* site). The centre shift values are reported relative to α -iron at ambient conditions. Iron cations in two crystallographically distinct sites in the garnet structure may have different recoil-free-fractions (*f*-factors)^{37,38}. The Debye approximation was used to correct for the different *f*-factors, where values of the effective Debye temperatures for *X* and *Y* sites were taken from refs^{37,38}. Additional absorption in the JF-22A spectrum was fit to a quadrupole doublet and assigned to Fe²⁺ in clinopyroxene on the basis of the hyperfine parameters.

X-ray optical components at the ID18 beamline contain very small amounts (ppm level) of iron. Generally, this amount of iron does not affect SMS spectra due to the strong signal from the sample. However, due to the small size of the samples studied and the low natural abundance of ⁵⁷Fe, the signal from the sample was sufficiently weak that spectral contamination from iron in the X-ray optical components could be detected. To account for this effect at each experimental run (that is, for different combinations of X-ray optical components), SMS spectra were measured without any sample so that Mössbauer absorption due to the optical components could be accurately determined for each of the garnet SMS spectra.

The Mössbauer spectra of studied inclusions do not show the presence of Fe²⁺ in the *Y* site. This agrees with published results³⁹ that concluded that in majoritic garnet there is a strong preference to balance Si⁴⁺ in the *Y* site by Mg²⁺ (rather than Fe²⁺).

XRD. XRD measurements were performed at the Extreme Conditions Beamline P02.2 at PETRA III (Hamburg)⁴⁰. Data were acquired with a PerkinElmer XRD1621 flat panel detector, X-ray beam size 5 × 8 µm² (FWHM), and wavelength $\lambda = 0.29464$ Å. XRD 'wide-scan' images were collected during continuous rotation of the samples from -20° to +20° on the vertical goniometer axis (ω); single-crystal data collection experiments were performed by narrow 0.5° ω -scanning in the range from -35° to +35°. Data integration and absorption corrections were performed with CrysAlisPro⁴¹ software version 171.38.43. Refinement was performed using the JANA2006⁴² version from 25.10.2015.

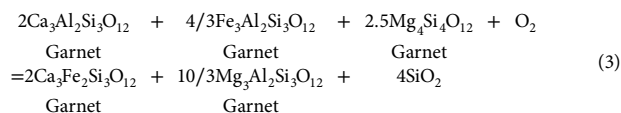
XRD data analysis. Analysis of diffraction patterns shows that all garnet inclusions studied are single crystals, mostly mono-domain, and only samples JF-58B and JF-22A contain more than two domains (but all with the same lattice parameters within measurement uncertainty). Within the detection limits of XRD, all samples except for three are monomineralic. Samples JF-44B and JF-58B show the presence of a small amount of polycrystalline phase(s) (strongest intensity of impurity powder diffraction lines are within 0.5% of the (420) diffraction line of garnet). Sample JF-84A contains single-crystal domain of clinopyroxene (space group *C2/c*, *a* = 9.650(4), *b* = 8.828(2), *c* = 5.2481(11) Å, β = 106.91(3)°, *V* = 427.8(2) Å³). However, its relative phase fraction is negligible and its presence does not affect the structure refinement of the XRD data. The contribution to the Mössbauer spectrum is negligible within the statistics of the data.

The structural analysis of garnets is a well-established method of studying the distribution of elements over different crystallographic sites. For this study the amount of iron in the different structural positions is particularly relevant. Accurate structure refinements provide an average atomic scattering factor in the different crystallographic sites, thus imposing constraints on the types and amounts of elements in the sites. Silicate garnets have the general formula $X^{2+}_3Y^{3+}_2(SiO_4)_3$ and crystallize in the cubic structure (*Ia* $\bar{3}d$ space group). The octahedral *Y* site is usually populated by a trivalent cation (Al³⁺, Fe³⁺, Cr³⁺) and at high pressure could accommodate (as in majorite) Si⁴⁺ (balanced by Mg²⁺, in particular). Divalent cations (Mg²⁺, Ca²⁺, Fe²⁺, Mn²⁺ and so on) occupy the distorted *X* site. Natural samples have complex chemical compositions. Even if one

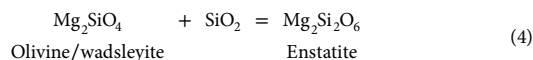
assumes that the contributions by Na, Mn, Cr and Ti to diffraction intensity are negligible (total up to ~3 at% in some samples), it is not possible to simultaneously refine the occupancies of four different atoms (Mg, Fe, Al, Si) in the *Y* site and three atoms (Ca, Mg, Fe) in the *X* site. Based on the known crystal chemistry of silicate garnet, all structural positions may be assumed to be fully occupied and charge (valence) balanced. Unambiguous refinements of iron occupancy in the *X* and *Y* sites are not possible and require information about the amount of other components from chemical analysis. We tested different combinations of constraints for sample JF-22a, and all give the same outcome within uncertainty (~0.5%). In the final model, we performed structural refinements of all garnets with the following composition constraints: (i) each crystallographic site of garnet is fully occupied, (ii) only O, Si, Mg, Al, Fe and Ca are considered and the presence of other elements is neglected, (iii) in the *Y* site, Mg, Si and Al are refined as a single 'Al' atom (X-ray scattering by equiproportional mixture of Si and Mg approximately the same as scattering by Al) and (iiii) the amount of Ca in the *X* site is fixed based on the microprobe data.

Overall, there is good (within 3 σ) agreement between determinations of Fe³⁺ content in all garnets studied by Mössbauer spectroscopy and XRD as well as with calculations based on the composition assuming stoichiometry (Supplementary Table 4). We note that the Fe³⁺ content derived from Mössbauer spectroscopy is systematically higher than the amount obtained from XRD data. The reasons for this minor inconsistency could be simplifications (assumptions) made during the structural refinements and/or complications in the analysis of overlapping components in SMS spectra (in particular the impurity signal from iron in the X-ray optical components).

Thermodynamic calculations. All end-member thermodynamic data for our calculations, except that of the IW reaction, were taken from the literature^{21,22}. We used the equilibrium:



to estimate the oxygen fugacities at which the garnet inclusions were formed. As the inclusions do not contain a SiO₂ phase we need to estimate the activity of this component. We approximated this activity using end-member data for the reaction:



Coexistence of olivine and enstatite, as in a mantle peridotite, defines the activity of SiO₂. In this case we used stishovite as our SiO₂ end member so that SiO₂ activities are expressed relative to this standard state. As we do not observe olivine and orthopyroxene in the garnet inclusions we arbitrarily raised SiO₂ activity by 0.01 log units relative to olivine (wadsleyite above 13 GPa) stability.

Using a standard state of the pure phase at the pressure and temperature of interest we followed published methods⁴³ to compute activities of the Ca₃Al₂Si₃O₁₂, Fe₃Al₂Si₃O₁₂, Mg₃Al₂Si₃O₁₂ and Ca₃Fe₂Si₃O₁₂ components from the compositions of the garnet (gt) inclusions. For the majorite component Mg₃Si₄O₁₂ we computed activities (*a*) from the garnet compositions using two possible expressions:

$$\begin{aligned} RT \ln a_{\text{Mg}_3\text{Si}_4\text{O}_{12}}^{\text{gt}} &= RT \ln 4x_{\text{Mg}}^{\text{c}}x_{\text{Si}}^{\text{o}2} + RT \ln \gamma_{\text{Mg}_3\text{Si}_4\text{O}_{12}}^{\text{gt}} \\ RT \ln a_{\text{Mg}_3\text{Si}_4\text{O}_{12}}^{\text{gt}} &= RT \ln 4x_{\text{Mg}}^{\text{c}}x_{\text{Mg}}^{\text{o}}x_{\text{Si}}^{\text{o}} + RT \ln \gamma_{\text{Mg}_3\text{Si}_4\text{O}_{12}}^{\text{gt}} \end{aligned} \quad (5)$$

In equation (5), *R* is the universal gas constant, *T* is the temperature, x_{Mg}^{c} , x_{Mg}^{o} , x_{Si}^{o} refer to the atomic fractions of Mg and Si in the cubic (c) and octahedral (o) sites and the factor 4 normalizes so that pure Mg₃Si₄O₁₂ has activity 1.0. The first expression assumes stoichiometric substitution of Mg₃Si₄O₁₂ into garnet so that there are equal mole fractions of Mg and Si on the octahedral site. The second expression is more realistic in allowing for different fractions of Mg and Si on the octahedral sites, but is impossible to compute exactly because the partitioning of Fe²⁺ and Mg between cubic and octahedral sites cannot be determined exactly by either stoichiometry or XRD.

The activity coefficient, $\gamma_{\text{Mg}_3\text{Si}_4\text{O}_{12}}^{\text{gt}}$ was calculated using the regular solution parameters from a previous study²¹. Note, however, that these contain no reciprocal terms⁴³ and no terms involving Fe³⁺.

We used our analyses to assign atoms to sites in the normal way:

Cubic: Ca, Mg, Fe²⁺, Mn

Tetrahedral: Si

Octahedral: Al, Cr, Fe³⁺, excess Si from tetrahedral and excess (Mg+Fe²⁺) from cubic.

We then computed activities using both expressions (5) and, since the octahedral site is smaller than the cubic site assumed either that all of the excess cubic site atoms were Mg (smaller than Fe²⁺) or that they were 75% Mg and 25% Fe²⁺. Use of the first activity expression in equation (5) yields the highest oxygen fugacities and it is these,

which are shown on Fig. 3. Use of the second expression with all 'excess' cubic atoms as Mg yields values on average $0.6 \log f_{\text{O}_2}$ units lower, while the allocation of 75% of the excess cubic atoms to Mg and 25% to Fe^{2+} means that average oxygen fugacities are $0.9 \log f_{\text{O}_2}$ units lower than shown. However, the addition of activity coefficient terms, currently unknown, for octahedral site interactions involving Mg, Si and Fe^{3+} would, we believe, tend to shift calculated oxygen fugacities to values higher than shown. Hence we consider that the simpler activity expression of equation (5) provides a reasonable compromise. In support of this conclusion we observe that 4 of the 5 iron metal-saturated experiments in a previous study²⁰ plot correctly in the Fe stability field of Fig. 3 and that only one of our 13 inclusions plots just into the Fe stability field. It should also be noted that, although the absolute uncertainties must be of the order of 1 log unit in f_{O_2} , errors in the activity expressions would shift all points up and down by similar amounts, thus preserving the trends observed in Fig. 3. Relative uncertainties are thus estimated by the differences in calculated f_{O_2} between the majorite inclusions and the published Fe-metal saturated experiments²⁰ shown in Fig. 3. Relative uncertainties must be about ± 0.3 log units or less to preserve the clear distinctions between the two sets of data.

Data for the IW buffer⁴⁴ at 1 atmosphere were fitted to $1/T$ to enable extrapolation to high temperature. They were extrapolated in pressure using the Murnaghan equation of state with volumes, thermal expansion coefficients and bulk moduli⁴⁵.

Data availability. CCDC entries 1588374 to 1588386 contain the supplementary crystallographic data for this paper. The data can be obtained free of charge from the Cambridge Crystallographic Data Centre via www.ccdc.cam.ac.uk/structures. The Mössbauer spectra and the thermodynamic calculations are available from the corresponding author upon request.

References

33. Potapkin, V. et al. The ^{57}Fe synchrotron Mössbauer source at the ESRF. *J. Synchrotron Radiat.* **19**, 559–569 (2012).
34. Nestola, F. et al. Synchrotron Mössbauer source technique for in situ measurement of iron-bearing inclusions in natural diamonds. *Lithos* **265**, 328–333 (2016).
35. Prescher, C., McCammon, C. & Dubrovinsky, L. MossA: a program for analyzing energy-domain Mössbauer spectra from conventional and synchrotron sources. *J. Appl. Crystallogr.* **45**, 329–331 (2012).
36. Geiger, C. A. et al. A combined temperature dependent ^{57}Fe Mössbauer and single crystal X-ray diffraction study of synthetic almandine: evidence for the Goldanskii–Karyagin effect. *Phys. Chem. Miner.* **19**, 121–126 (1992).
37. Lyubutin, I. & Dodokin, A. Temperature dependence of Mössbauer effect for Fe^{2+} in dodecahedral coordination in garnet. *Sov. Phys. Crystallogr.* **15**, 1091–1092 (1971).
38. Lyubutin, I., Dodokin, A. & Belyaev, L. Temperature dependence of Mössbauer effect for octahedral iron atoms in garnets. *Sov. Phys. Solid State* **12**, 1100–1101 (1970).
39. McCammon, C. A. & Ross, N. L. Crystal chemistry of ferric iron in (Mg, Fe) $(\text{Si,Al})\text{O}_3$ majorite with implications for the transition zone. *Phys. Chem. Miner.* **30**, 206–216 (2003).
40. Liermann, H. P. et al. The extreme conditions beamline P02.2 and the extreme conditions science infrastructure at PETRA III. *J. Synchrotron Radiat.* **22**, 908–924 (2015).
41. CrysAlisPro v.171.38.43 (Agilent Technologies, 2013).
42. Petříček, V., Dušek, M. & Palatinus, L. Crystallographic computing system JANA2006: General features. *Z. Krist. Cryst. Mater.* **229**, 345–352 (2014).
43. Stagno, V., Ojwang, D. O., McCammon, C. A. & Frost, D. J. The oxidation state of the mantle and the extraction of carbon from Earth's interior. *Nature* **493**, 84–88 (2013).
44. Holmes, R. D., O'Neill, H. S. C. & Arculus, R. J. Standard Gibbs free energy of formation for Cu_2O , NiO , CoO , and Fe_3O_4 : High-resolution electrochemical measurements using zirconia solid electrolytes from 900–1400 K. *Geochim. Cosmochim. Acta* **50**, 2439–2452 (1986).
45. Ahrens, T. J. (Ed.) *Mineral Physics and Crystallography: A Handbook of Physical Constants* (American Geophysical Union, Washington DC, 1995).